Astron. Astrophys. 308, 957–969 (1996)

ASTRONOMY
AND
ASTROPHYSICS

Subflares and surges in AR 2744 during the Solar Maximum Mission

B. Schmieder[1], M. Rovira[2], G.M. Simnett[3], J.M. Fontenla[4], and E. Tandberg-Hanssen[5]

[1] Observatoire de Paris, Section de Meudon, URA 326, F-92195 Meudon Principal Cedex, France
[2] IAFE, CC67, Suc. 28, 1428 Buenos Aires, Argentina
[3] The University of Birmingham, Space Research, Edgbaston, Birmingham B15 2TT, UK
[4] HAO/NCAR, P.O.Box 3000, Boulder, CO 80027, USA
[5] Space Science Division, Marshall Space Flight Center, Huntsville, AL 35812, USA

Received 4 April 1995 / Accepted 22 August 1995

Abstract. Active region NOAA 2744, which was at S25, had its central meridian passage on Oct 23 1980 and was relatively quiet according to Hα, UV and X-ray observations made by the Solar Maximum Mission (SMM). The region was also observed by the Marshall Space Flight Center (MSFC) vector magnetograph. During its disk passage only subflares and surges were detected. Their locations appeared to be governed by the magnetic topology. On October 21 a miniflare occurred close to the separator between the two main sunspots. On October 22 the emergence of a small region of parasitic polarity in the existing magnetic field appeared to be responsible for three subflares and subsequent surges. We discuss the energy budget for plasmas at temperatures in the 10^4 K, 10^5 K and 10^6 K ranges in the context of surge-trigger mechanisms. On October 21 the energy deposition driving the surges did not produce a high temperature plasma. By October 22 the active region had evolved and the surges were now associated with some high temperature plasma. However, the energy radiated at transition region temperatures would be larger than that estimated in X-rays depending on the dilution factor. This would imply a continuous influx of energy in order to sustain the long duration surge (30 min) rather than a simple, impulsive energy input. If the electron density in the 10^4–10^5 K plasma is taken as $\sim 10^{12}$ cm^{-3} the diameter of individual surge loops should only be $\sim$ 40 km. The relevance of our results to (a) reconnection and (b) gradient pressure driven models for surges is discussed.

Key words: Sun: activity – flares – X-rays

1. Introduction

Chromospheric mass ejections, called surges when viewed in the Hα line, are not necessarily associated with flares. Even when they occur simultaneously with flares their physical association is controversial. Some large ejections are directly related to flares (Simnett et al. 1990) or coronal jets (Shibata et al. 1992a). Other surges may be associated with weak enhancements in soft X-ray emission, where the X-ray radiative energy is low, by 2 orders of magnitude, compared with the kinetic energy (Schmieder et al. 1988). Shibata et al. proposed that the coronal electron density is very low around the surge – 10^9 cm^{-3} – and this makes it relatively invisible as a jet. Schmieder et al. suggested that flares and surges are signatures of energy release in structures of different nature. Surges are observed when the energy release is mainly transferred to mechanical energy in an open structure, whereas flares or X-ray-associated surges occur if a significant amount of energy goes into magnetically-closed structures, where the energy is efficiently contained, thus allowing the temperature to rise. This may also require the rate of energy dissipation in the chromosphere to be high, to combat the effects of cooling.

The physical mechanisms which are involved are not clearly understood. The surge may be driven by a high pressure gradient in a magnetic tube, as first proposed by Steinolfson et al. (1979) or it may be due to magnetic energy release in a more complicated structure through reconnection (Heyvaerts et al. 1977; Shibata et al. 1992b). In the first case we would expect substantial pre-heating of plasma, while in the second case restructuring of the magnetic field should occur following a heated bright point. The latter would indicate where the reconnection takes place.

In one surge Schmieder et al. (1994) ruled out the pressure gradient model because the X-ray emission, observed with the Normal Incidence X-ray Telescope (NIXT), was two orders-of-magnitude lower than that needed for the high pressure region to drive such cold plasma ejection. Shibata et al. (1992a) showed that X-ray emission and ejected cold plasma do not follow the same magnetic field lines so a gradient of pressure in a magnetic flux tube cannot be considered a possible mechanism. Both Schmieder et al. (1995) and Shibata et al. (1992b)

Send offprint requests to: B. Schmieder

have proposed a reconnection model, supported by direct observations with *Yohkoh*. If the reconnection occurs in the deep chromosphere, the energy release will tend to heat plasma more to transition region temperatures than X-ray emitting temperatures, which should be detectable in UV lines. This could be tested by using surge observations in multi-wavelengths.

In this paper we study the conditions for flares and surges in active region (AR) 2744 on October, 21 and 22 1980 using observations from SMM and coordinated ground-based observations, which together cover a wide temperature range from $< 10^4$ K to $> 10^7$ K. We relate these data to the magnetic field structure inferred from the vector magnetograms and to magnetic field extrapolations. For several of the surge events, especially the large surge of October 22, we have estimated the amount of the energy release versus time and according to the temperature range. Finally we discuss the two possible surge-driver mechanisms.

2. Observations

2.1. Instruments

During the internationally-coordinated Flare Build-up Study (FBS) in 1980 several active regions were followed with a wide variety of instrumentation. For the present study we used the following data:

(a) Debrecen Observatory provided white light photographs and filtergrams in different wavelengths around the Hα line.

(b) The Multichannel Subtractive Double Pass (MSDP) spectrograph, operating on the Solar Tower of Meudon, provided images of an elementary field-of-view ($1' \times 8'$) in 9 channels in the Hα line. The profile of the line was reconstructed for all the image pixels, from which maps of intensity and Doppler-shifts were derived.

(c) The Ultra-Violet Spectrometer and Polarimeter (UVSP) on SMM provided large rasters of 80 × 80 pixels followed by small rasters 40×40 pixels with a spatial resolution of 3″. These data are recorded by two detectors simultaneously: one is centered in the 153.34 nm Si II line ($T \sim 3 \times 10^4$ K) and one in the 154.8 nm C IV line ($T \sim 10^5$ K). For the coalignment with the optical data we used the following experiments: No.14202 at 16:34 UT (C IV) and No.14207 at 18:20 UT (continuum).

(d) The Hard X-ray Imaging Spectrometer (HXIS) on SMM observed in the energy range 3.5–30 keV with a coarse field of view (32″ resolution) of $\sim (6'24'')^2$ and a fine field-of-view (8″ resolution) of $\sim (2'40'')^2$.

(e) The Marshall Space Flight Center (MSFC) provided vector magnetic field data of which mainly the longitudinal component was used.

Table 1 shows the observation times of AR 2744 for the different instruments; for the UVSP the numbers of the experiments performed are also given.

2.2. Topology of the active region

Active region 2744 consisted of two quasi-regular bipolar sunspot groups with two leading spots of negative polarity, one with a following positive sunspot and the other with a facu region (Kovács & Dezsö 1988). East of the group there w another active region 2748 with a large round spot. Kovács a Dezsö reported that the spot motions of AR 2744 revealed o the usual drift during the whole disk passage and that no i portant events were observed. Nevertheless a certain number interesting subflares and surges appeared from time to time listed in Table 2.

Table 1. Summary of the observations

	Time in UT	
Data from	October 21	October 22
Debrecen	06:00–14:00	08:00–14:00
MSDP	08:15–13:52	08:19–09:03
UVSP	14085 08:39–14090 09:31	14176 08:35–14181 09:
		14183 10:11–14188 11:
		14190 11:46–14192 12:
	14106 13:27–14111 14:19	14194 13:22–14196 13:
		14202 16:34–14207 18:
HXIS	08:31–09:34	08:35–09:27
	10:08–11:12	10:11–11:03
	11:42–12:09	11:46–12:05
	12:28–12:45	13:22–13:41
	13:17–13:44	13:00–13:38
	14:14–14:23	14:24–15:18
MSFC	no	14:41

Table 2. Events observed at Meudon (M) or at Debrecen (D)

Day	Time in UT	Events
Oct. 21	08:40, 09:02	Small surges around the leading sp (M and D)
	11:40, 12:45, 13:50	Bright points between the leadi spots (M)
Oct. 22	13:35	Subflares in the western side of t leading spots (D)
	13:33, 13:40	Surges (D)

2.3. Magnetic field and position of the kernels

The main events occurring on October 21 and October 22 n be due to the emergence of new flux as we will show bel We have used the magnetogram of MSFC of October 22 both days. In Fig. 1a and b we can see a weak (10^{-3} T) posit parasitic polarity (P) immersed in a strong negative field. have to take into account that the methods used by the MS magnetogram to reduce the data have some uncertainties du the fact that it measures a flux over a fixed area. If concentra polarity of one sign is surrounded by the opposite polarity, magnetic field of the parasitic polarity will be underestimat

Between the magnetograms on two consecutive days parasitic polarity was growing in size and intensity, and an contour of 5 10^{-3} T became clearly identifiable by 13:32

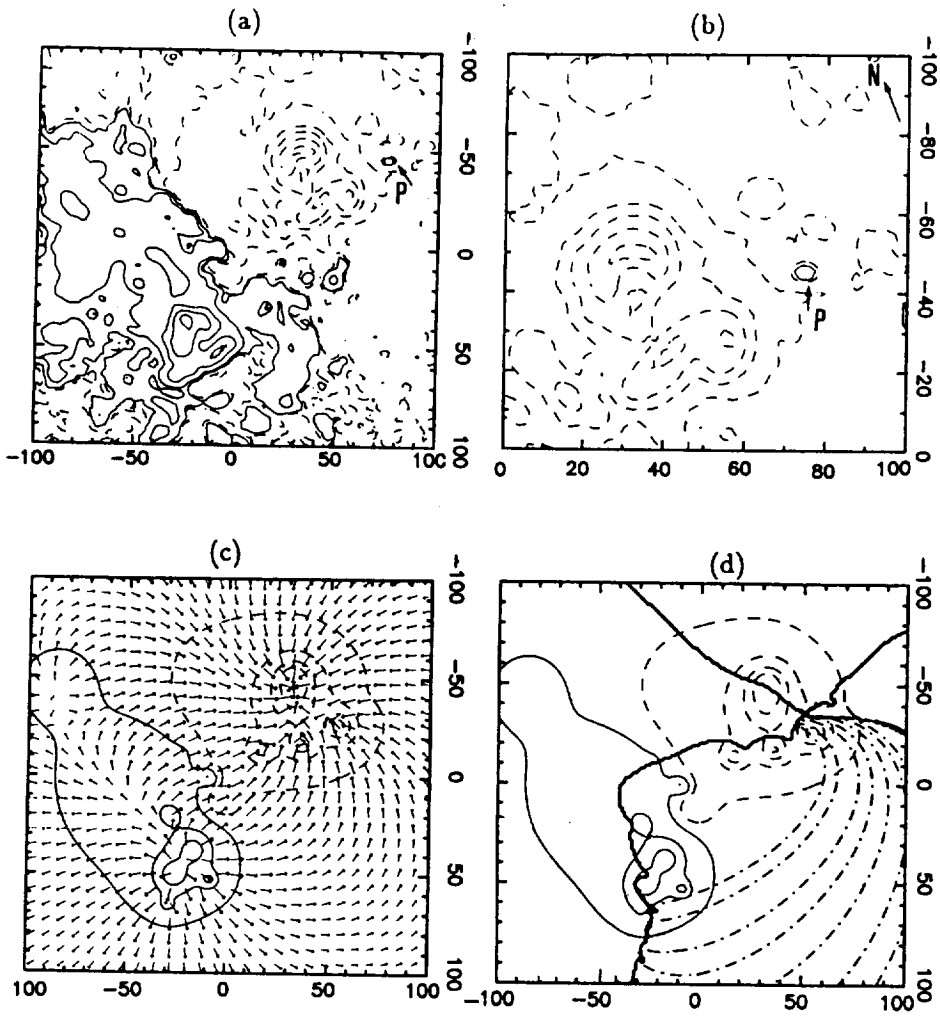

Fig. 1a–d. **a** Observed longitudinal magnetic field of AR 2744 obtained by MSFC at 14:41 UT on October 22, 1980. Continuous (dashed) lines are for positive (negative) values. The isocontour levels are ±0.001, 0.01, 0.05, 0.1, 0.15, 0.2 T. In all these figures the spatial scale is in Mm. The letter P indicates the parasitic polarity immersed in strong negative polarity. **b** an enlargement of the region around P. **c** Horizontal and longitudinal magnetic field at the photospheric level computed with a linear force-free field assumption ($\alpha = -0.006\,\mathrm{Mm}^{-1}$). Nine magnetic dipoles (18 sources) are used for the model. Their depths and intensities are computed by fitting the model with the observed longitudinal field of October 22. The longitudinal magnetic field isocontour levels are: ± 0.01, 0.05, 0.1, 0.15, 0.2 T. **d** Intersection of separatrices with the photospheric plane (thick lines) and computed vertical magnetic field (dashed and thin lines). The isocontour levels are ± 0.001, 0.01, 0.05, 0.1 T. Magnetic field lines projected on the photospheric level (dash-dot) follow a path very similar to that of the observed surges

October 23. We identify this growing positive magnetic field, located very close to the origin of the sub-flare, as the trigger for the energy release (see Sect. 4.1). This observation has some similarity with those presented by Mandrini et al. (1993) and Démoulin et al. (1994).

As in previous works (Démoulin et al. 1994 and van Driel-Gesztelyi et al. 1994) we modeled the coronal magnetic field by an ensemble of sub-photospheric sources whose positions and intensities were deduced from a least-squares fit between the computed and observed longitudinal magnetic fields. Eighteen sources were sufficient to produce a satisfactory fit. For AR 2744 a linear force-free extrapolation was used to take into account the departure from a potential field ($\nabla \times \boldsymbol{B} = \alpha \boldsymbol{B}$). The value of $\alpha = -0.006\,\mathrm{Mm}^{-1}$ was determined by comparing the average observed direction of Hα fibrils in the region of interest with the calculated transverse field.

It is important to note the limitations of the linear force-free modeling. First, a constant alpha imposes a vertical current density j_z which is proportional to the observed vertical field B_z. Second, a constant alpha gives only a representation of the average shape of the fibrils; and third, only the field lines longer than α^{-1} are affected by the field-aligned currents. However, since the linear force-free approximation is the only available model of a non-potential 3D field, we have employed it here. As our field-of-view covers 200 Mm, the chosen α value implies a scale length for the shear of 159 Mm which seems reasonable for our spatial scales.

Figure 1c shows the adjusted magnetic field and the computed topology. In Fig. 1d, we have drawn the intersections (solid lines) of the separatrix with the photosphere. The point where the solid lines cross is close to where the sub-flare of October 21 took place (see Sect. 3). We have also drawn the magnetic field lines (dashed-point lines) starting at this point. Note the strong similarity between these coronal field lines and the paths followed by the surges on October 22 observed in Hα (see Sect. 4). Figure 2 shows the relative position of the SMM instruments and the magnetogram of the active region with the heliographic north oriented vertically. The HXIS coarse field-of-view is the large square with the corners missing. The main raster of UVSP is the large square at the same orientation as the X-ray image; within this square is shown the position of the

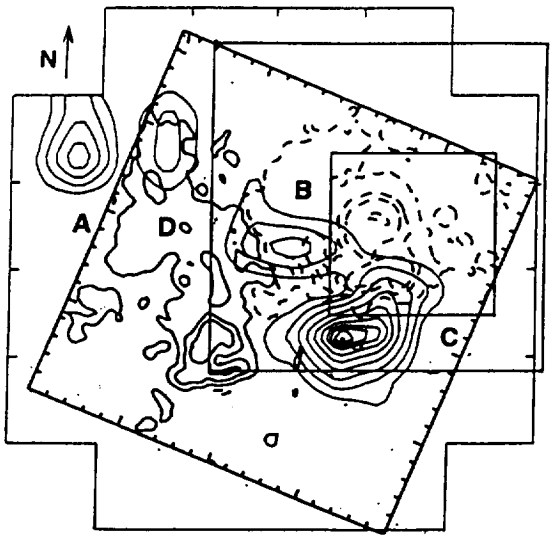

Fig. 2. The 3.5–5.5 keV X-ray image from 08:34–09:00 UT on October 21. The relative position of the large raster of UVSP is the large square at the same orientaion as the X-ray image; within this square is shown the position of the UVSP small (120″×120″) raster used between 08:40 and 10:15 UT. The locations of the four X-ray sources are marked A-D. Superimposed on the image is the magnetogram of the active region (square at a different orientation) with the positive field shown as solid contours

UVSP small (120″ × 120″) raster between 08:46 and 10:15 UT on October 21.

3. Subflares and ejecta of October 21

3.1. Hα and UV observations

Figure 3a shows a white-light image of the active region on 21 October, 1980, and Fig. 3b shows an Hα image taken at 08:40:52 UT. The square box indicates the position of the UVSP 4′ × 4′ raster. The positions of the three sunspot groups which we identify are shown as I, II and III. From 08:40 to 09:02 UT around the leading spots, dark fibrils or small radial ejecta were detected with typical bright signatures at their feet in Hα line center (indicated by the letter S and arrows in Fig. 3b). The ejecta are better seen in Hα wing images (not displayed in this paper), due to high velocities. The magnetic field map (Fig. 1b) shows no features corresponding to those in Hα, but the spatial resolution may have been too low to detect small parasitic polarities around the sunspots. In the facula C, indicated in Fig. 3b at the southern group, we observed some brightness in the wing of Hα that we interpret as a miniflare.

Later (clearly visible at 11:43 UT), a recurrent miniflare appeared between the two leading spots (Fig. 3c). In the Si II images the sunspots appear as dark areas, while the Hα faculae correspond to bright areas (see for example the arrow S in Fig. 4). The C IV images give a snapshot of the active region in a transition zone temperature.

Four bright points around the leading spots observed in C IV (Fig. 4a) match the four feet of the ejecta observed in Hα (Fig. 3b). They are obvious in the 08:40:52 UT picture and persisted until 09:27 UT. Such brightening in transition zone lines corresponding to surges has been already observed with UVSP instrument (Schmieder et al. 1983).

At that time another brightening appeared between the spots, apparently lasting until the end of the observations at 14:15 UT. However, the two main spots are not in the field-of-view covered by the small raster between 10:15 and 13:27 UT. The miniflare between the two spots was visible before and after this period. If we coalign the C IV image to the magnetic field map using Fig. 2, we see that the miniflare is located at the intersection of the 2 separatrix traces on the photosphere (Fig. 1d). The maximum C IV intensities occurred at 13:45:51 and 14:08:09 UT (Fig. 4b). The bright facula in Hα corresponds to a bright region in C IV.

3.2. X ray emission

Figure 2 includes a 3.5–5.5 keV X-ray image taken from 08:34:50 to 08:59:43 UT. This image has four distinct X-ray features which we have labelled A, B, C and D. Here the maximum in feature C corresponds to the location of facula C with the resolution of HXIS. The X-ray emission occurred either in the vicinity of facula C, in the middle of AR 2744 (point B) or/and in some eastern points near the other sunspot group AR 2748 (A and D). A and D are outside the large UVSP rasters, and B and C are outside the small UVSP rasters.

Figure 5 shows the intensity-time profiles for the emission of regions A, B, and C from 08:30 to 09:35 UT. There was a small flare from C which was decaying in intensity when the observations started at the beginning of the SMM orbit at 08:34:50 UT; this start accounted for the apparent sudden rise in intensity seen in Fig. 5. For around 8 minutes centered at 08:39 UT there was an extremely soft X-ray enhancement from region D (Fig. 2) which was unrelated to other X-ray features other than that the decay was approximately coincident with the onset of the emission from region B. Similarly, as the emission from B started to decline, so that from A increased. The burst from A was remarkable in that the first part of the burst contained significant emission in the 5.5–8.0 keV energy band, whereas the last five minutes of the burst had no higher-energy photons above background. The remainder of the SMM orbit contains little of note, other than a hint of a correlated enhancement around 09:25 UT from regions A and B.

Between 13:17 and 15:00 UT there was very little activity. However at 14:15 UT there was a small burst in the east part of the region (A) and a weak response in B.

Table 3 shows the results of a temperature and emission measure analysis performed on the X-ray data. There is no evidence of any very high ($T > 10^7$ K) temperature component in these events, with the exception of a weak signal, but above background, from region B. Note however that the emission measure is only $1.4\ 10^{44}\ cm^{-3}$. Apart from this the plasma temperatures from regions B and D are 6.9 and 5.5 10^6 K respectively. A temperature of 5.5 10^6 K is close to the lower limit of temperatures that HXIS can measure. This sensitivity limit can generally only be reached if the emission measure is relatively

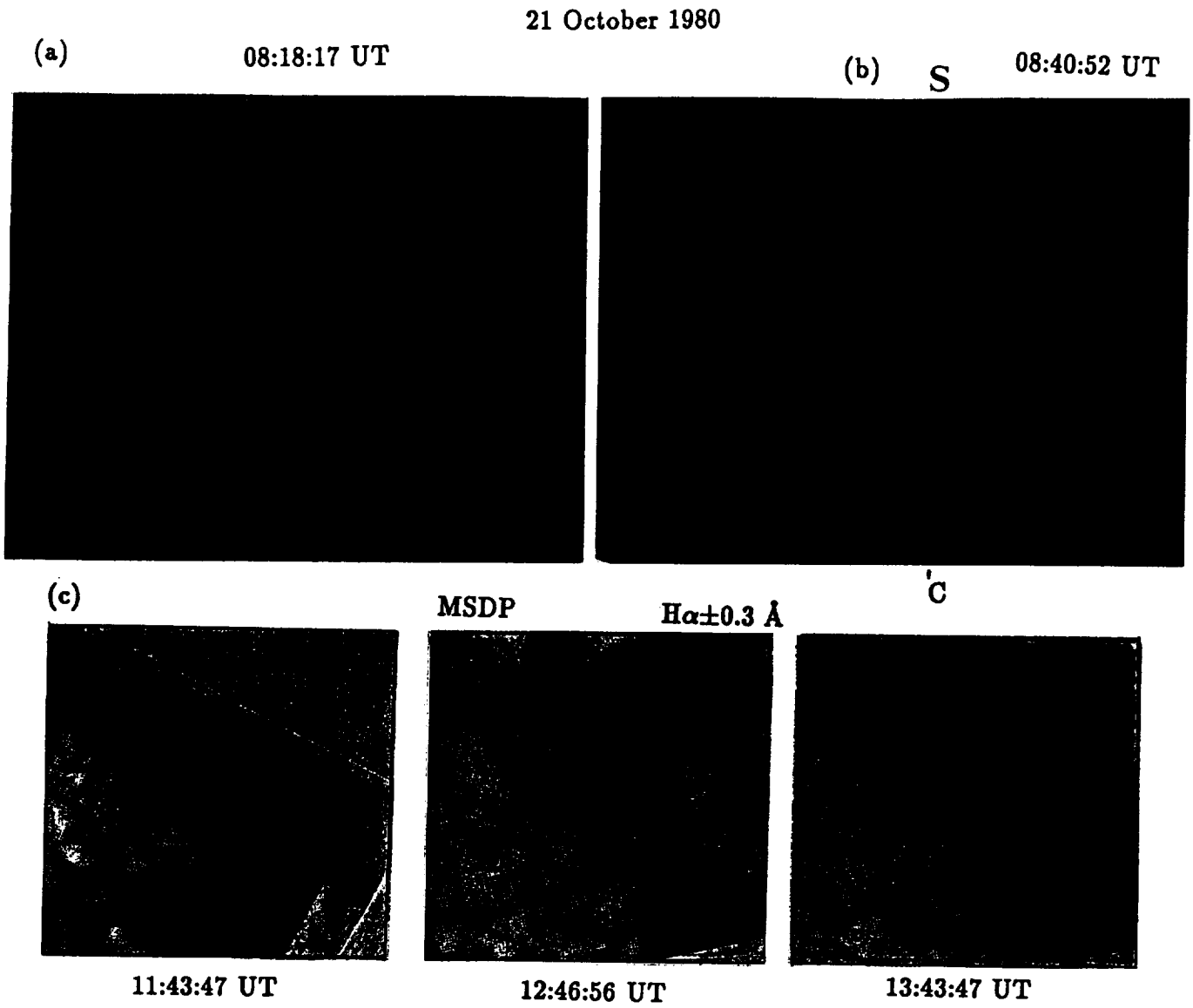

Fig. 3a–c. Observations of the AR 2744 (sunspot groups I and II) and AR 2748 (sunspot group III) on October 21. **a** White light image from Debrecen and **b** Hα image from Debrecen showing the facula C, bright points and dark fibrils (ejecta) around the leading spot I (arrows S). **c** MSDP: note the evolution of the miniflare between the two spots. The box represents the 4′ × 4′ UVSP raster

large, in this case 67 10^{46} cm^{-3}. We divide the burst from A into two parts, according to whether there was any detectable emission above 5.5 keV, or not. It seems that there was a relatively compact source at the start of the burst which was heated to a temperature around 11.7 10^6 K, which then rapidly cooled to 6.9 10^6 K. During the cooling the emission measure rose, which suggests that the source had expanded into a larger volume or that it had been cooled by the addition of fresh, cold, plasma.

There were type III radio bursts (Solar Geophysical Data) reported in time-coincidence with the events from D and B, but not from A. This could mean that the energy associated with A was more effectively contained in the very low corona than that associated with D and B, hence explaining the higher temperature of A.

3.3. Correlation between the surges and X-ray activity

The surges were observed from the north-western edge of facula C, whereas the impulsive, coincident X-ray activity came from points B and A. It would appear that there was energy input at chromospheric level in all these points, but that only in B and A was the energy deposition sufficiently contained, or over a sufficiently compact area, for the plasma temperatures to reach above 5.5 10^6 K. At the time of the surge the highest temperature in the X-ray emitting plasma was seen from points A and B, which were well-separated from C. Thus in this instance the energy deposition driving the surge did not produce a high temperature plasma, and the energy deposition which produced the high temperatures did not produce significant upward mass motions of cool material. During the period 13:44–14:13

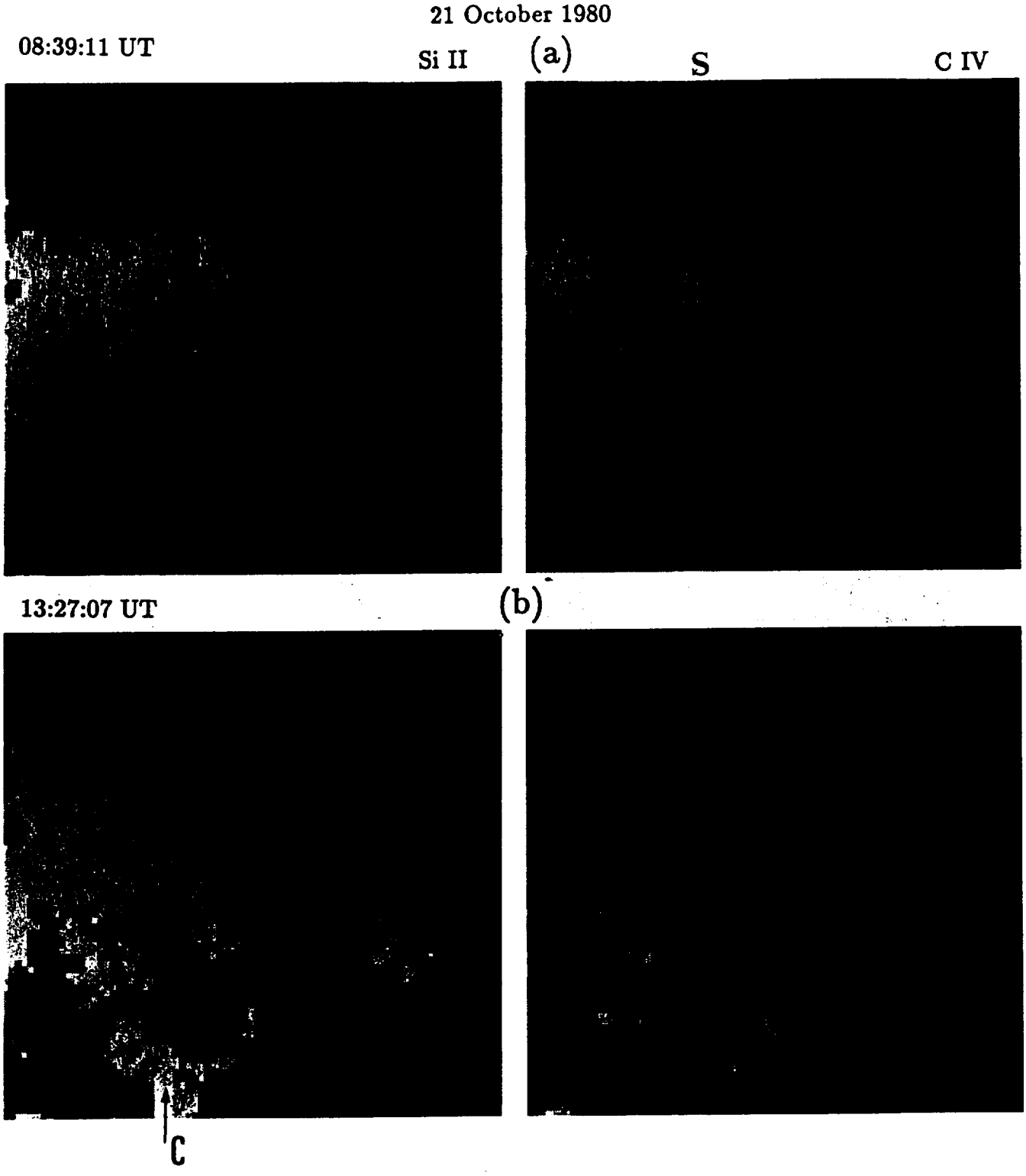

Fig. 4a and b. UVSP observations of the AR 2744 on October 21 in Si II and C IV. **a** Radial ejecta around the leading spot indicated by arr S, the bright area C corresponds to the Hα facula. **b** A miniflare between the two spots. North is towards the top of the page

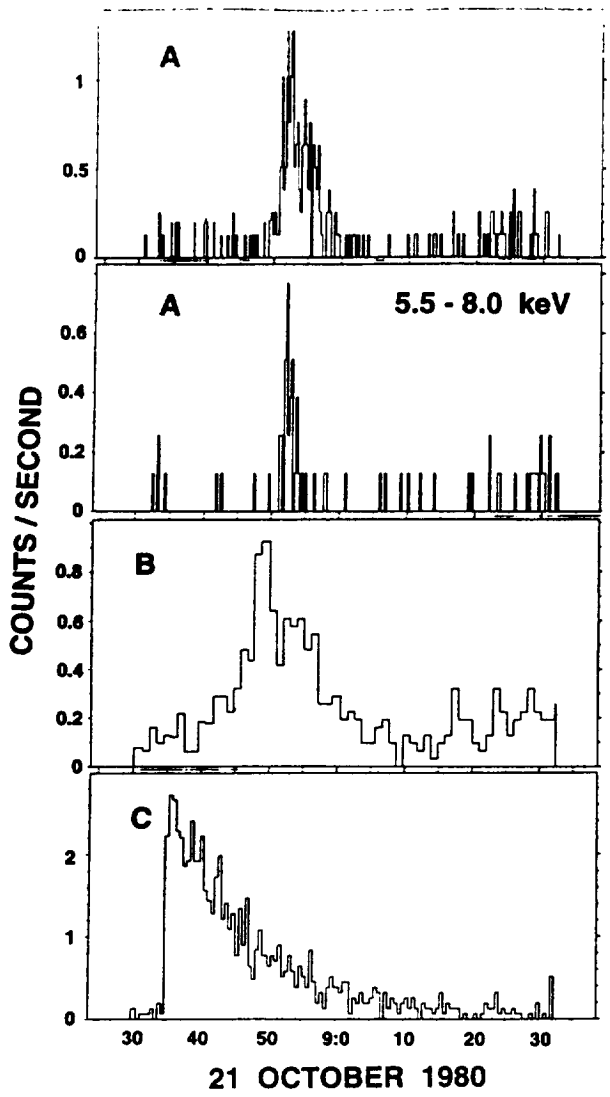

Fig. 5. HXIS 3.5–5.5 keV X-ray intensity-time profiles of points A, B, and C, indicated in Fig. 2, on October 21 from 08:30–09:32 UT; and for point A in the 5.5–8.0 keV energy band

UT HXIS was turned off due to the passage of the spacecraft through the South Atlantic Anomaly; however, the X-ray activity both before and after this period was from points B and A, and not from C, which was the site of the Hα activity. Thus for several hours the relationship between the surges and the high temperature plasma followed a consistent pattern.

4. Surge of October 22

4.1. Hα and UV

During the period of our observations the main Hα activity was an N-class flare at 13:35 UT on the western side of the region AR 2744 (E55). The first subflare was visible in Debrecen filtergrams at 13:32:58 UT in Hα +1 Å, and three subflares were detected in this area with maxima around 13:35 UT (Kovács & Dezsö 1990). Figure 6 shows two Hα – 0.5 Å images taken at 13:33:26 UT and 13:57:21 UT. The lines on these pictures represent the edges of the 4′×4′ UVSP raster. Almost simultaneously with the subflares we observed three surges which may have been flaring arches (Martin & Švestka 1988). A type III burst was recorded between 13:40 and 13:41 UT (Solar Geophysical Data). This time coincidence is consistent with that reported between type III radio bursts and surges from previous studies (Chiuderi et al. 1986). The surges lasted at least half an hour longer than the flare, which is clear from Fig. 6b. After flare onset, the surges were bright in Hα center near their bases until 13:36 UT. The trajectories of the surges were loop-shaped (Fig. 6b) and they reached their highest point by 13:45 UT. They correspond to the extrapolated magnetic field lines presented in Fig. 1 (dashed-point curves). They resemble those of "flaring arches", discussed further by Fontenla et al. (1991a). The true velocity after reconstruction of the loop geometry for this event was determined by Kovács & Dezsö (1990) and decreased from 150–200 km s^{-1} to 80 km s^{-1} at 13:45 UT with a deceleration 0.275–0.208 km s^{-2}. The surges were visible until 14:30 UT. At 13:55 UT the true length was around 150,000 km, and the apparent cross section was constant with a diameter of 5″ (4×10^3 km).

Figure 7 has eight parts. The upper two panels show large rasters in Si II and C IV obtained before the flares at 13:22 UT; the maximum number of counts in C IV was low (~ 400). Small rasters were taken at the following times in C IV and Si II simultaneously; six of them are displayed in the low panel of Fig. 7.

At 13:29:54 UT, around the onset of the flares, in both images the kernel has a circle-shape, although the intensity in C IV is much higher than in Si II. By looking at the coalignment of the observations that we proposed for October 22 in Fig. 8, we see that the UVSP small rasters contain the region of the parasitic polarity P, which is already present in the magnetic map (Fig 1b). Under close inspection the kernel seems to surround P.

At 13:33:37 UT, the time of the flare, the maximum count in C IV was >49,000, *i.e.*, about a factor 100 increase over the preflare level; it also extends to the south. At the lower temperature of the Si II line, the flare simply appears as two small bright points with some weak, diffuse emission under the main body of the flare plasma. The intensity decreased by the time of the third image at 13:37:20 UT, but the extension to the south now appears to be along a relatively thin path following the trajectories of the surges (Fig. 6b). This substantiates the relationship between the emerging flux P, the subflare and the surges.

Unfortunately the following satellite orbits did not contain useful data due to the passage of the spacecraft through the South Atlantic Anomaly.

4.2. X-ray flare at 13:35 UT

This flare reached a maximum around 13:35 UT. Fig. 8 shows a composite X-ray image of the region, where four X-ray bright points A, E, C′ and F are identified. The region is the same as that seen on October 21 (Fig. 2). Region A is essentially the same between Figs. 2 and 8. Region C′ has some overlap with region C, although the centroids of the emission are clearly different.

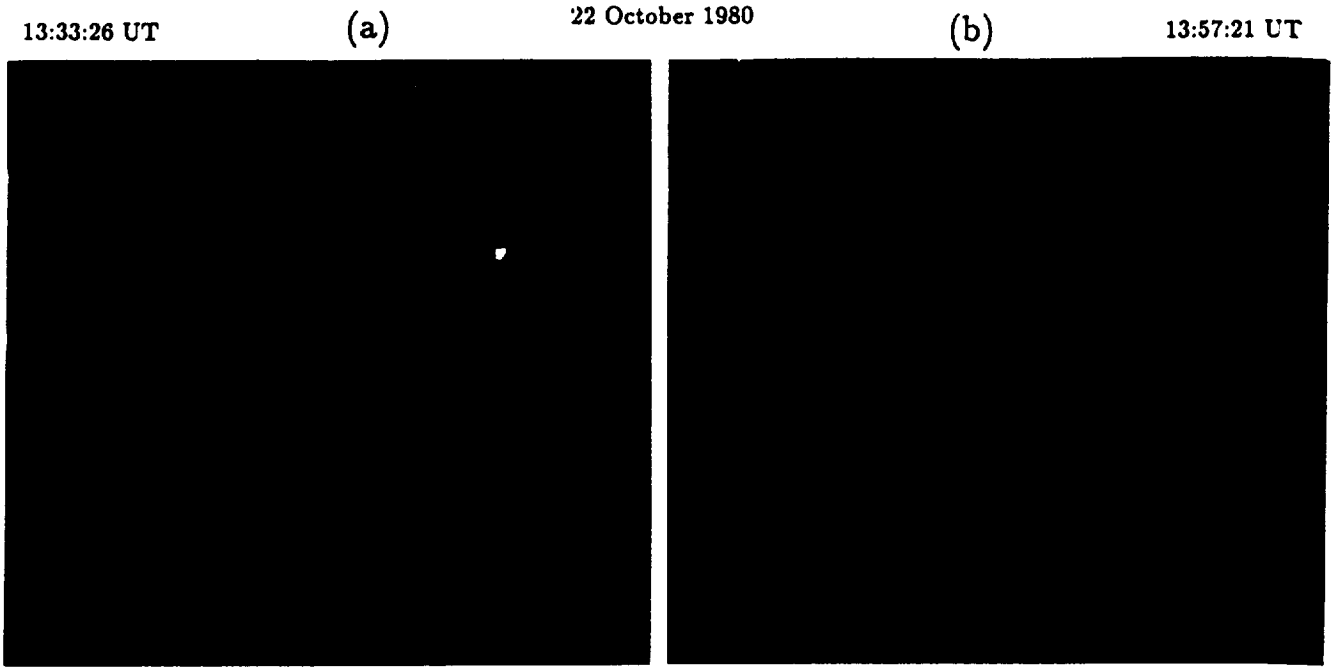

Fig. 6a and b. Debrecen observations of the AR 2744 on October 22 in Hα −0.5 Å. Note the subflares and the consequent surges in the western part of the two spots. The box represents the 4′ × 4′ UVSP raster. North is up

Table 3. Temperature and emission measure for the enhancements from regions A, B and D (see Fig. 2)

Region	Time interval Δt	Low temperature		High temperature	
	UT	T (10^6 K)	EM (10^{46} cm^{-3})	T (10^6 K)	EM (10^{46} cm^{-3})
A	08:51:40–08:53:58	11.7	5.0		
A	08:53:58–08:57:10	6.9	13		
B	08:44:51–08:58:11	6.9	29	30	0.014
D	08:37:33–08:41:11	5.5	67		

The fact that both C (Fig. 2) and C′ (Fig. 8) are the brightest features suggests that they are both connected to the main region of energy release. Two new points E and F are visible. In Fig. 8 the part of the image where points A and F are visible was taken from 13:31:57 to 13:35:12 UT, while the surrounding part of the image showing points C′ and E was taken between 13:37:10 and 13:38:19 UT. Figure 9 shows the intensity-time histories of the four points; A, E and F at 3.5–5.5 keV and C′ at 3.5–8.0 keV.

The main flare from point C′ clearly started no later than 13:33:30 UT, when the measured intensity exceeded 1 count/s; from the relative intensity of the soft X-rays, observed in the preceding 15 minutes, the increase became significant around 13:32:15 UT, when X-rays in excess of 11.5 keV were seen. Topologically the emission at point C′ (see Fig. 8) corresponds to the subflare observed in C IV (Fig. 7) and to the emerging flux detected as a parasitic polarity (Fig. 1b). Thus the high temperature plasma was seen near the base of the surge, which is opposite to the situation for the October 21 surge discussed above. One obvious difference is that the October 22 event involved much more energy deposition at C′. It is interesting to examine the intensity-time histories of the other points A, E and F. Region A, which was some 5′ to the east of C′ and is in AR 2748, started to brighten around 13:15 UT, and there was a very short spike at 13:22 UT. The main spike occurred at 13:34 UT, and the intensity was declining by 13:35 UT. Region E is even more interesting, in that the X-ray increase did not *start* until that from region C′ declined, and the maximum was reached about 13:37 UT. Region F brightened about the same time as A, but reached maximum intensity at 13:30 UT, definitely *before* any sign of an increase from the main flare site C′. Detailed comparison of the light curves from A and C′ shows that they have almost identical shapes, but A is an order-of-magnitude weaker, and leads C′ by 0.5–1.0 minutes. In all three regions there are significant counts in the 5.5–8.0 keV energy range. It seems reasonable that the delayed X-ray emission from E is a result of energy transport from C′. The connection from C′ to E suggests the existence of a closed magnetic structure, visible at both ends in soft X-rays (Fig. 8). This structure is not the same as the magnetic structure guiding the surge, but the two have adjacent footpoints in C′. The bright point C′ could be similar to tiny X-ray loops observed at the feet of open structures like surges and jets, as has been commonly observed with *Yohkoh/SXT* by Shibata et al. (1992a).

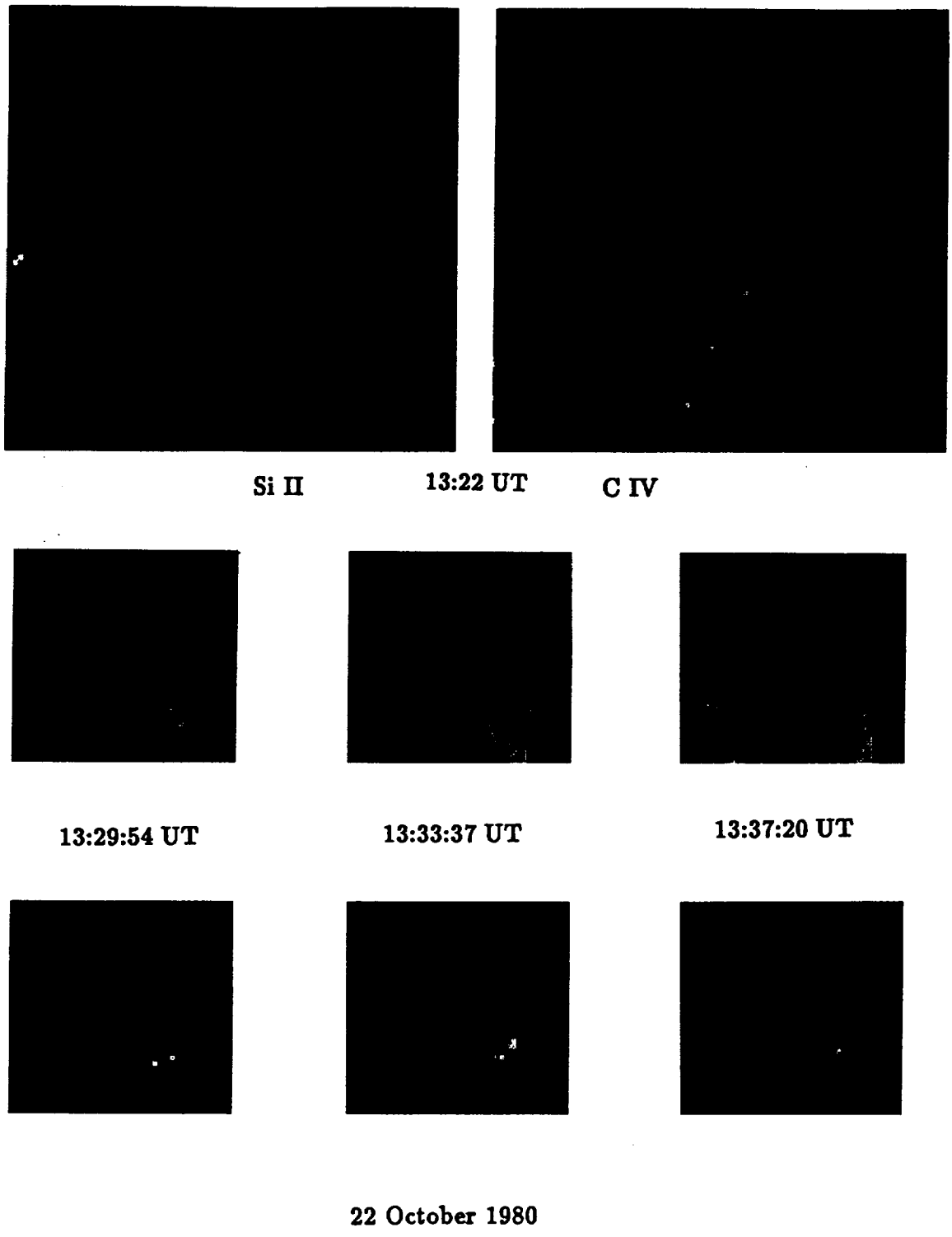

Fig. 7. UVSP observations of the AR 2744 on October 22 (a) C IV (b) Si II. Note the round-shaped C IV subflare at 13:29 UT and its extension to the south at 13:37 UT, corresponding to the Hα surge

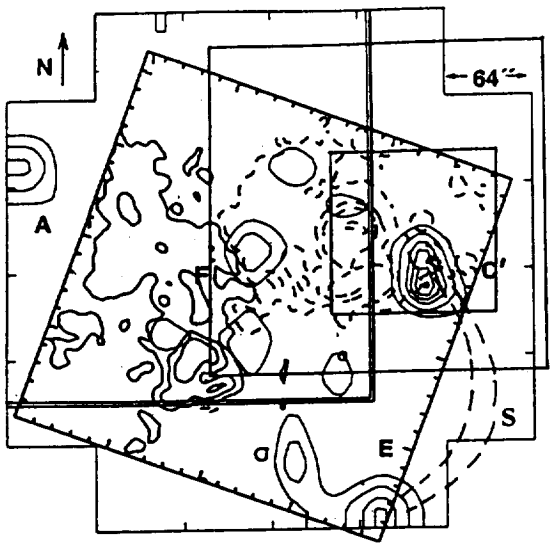

Fig. 8. A composite 3.5–5.5 keV X-ray image from 13:31:57 to 13:35:12 UT on October 22. The locations of the four X-ray sources are marked A, E, C′ and F. The points A and C′ correspond to similarly marked points in Fig. 2. The part of the image showing points A and F was taken from 13:31:57 to 13:35:12 UT, while the surrounding part of the image showing points C′ and E was taken between 13:37:10 and 13:38:19 UT. The relative position of the large raster of UVSP is the large square at the same orientation as the X-ray image; within this square is shown the position of the UVSP small (120″×120″) raster used between 08:46 and 10:15 UT. Superimposed on the image is the magnetogram of the active region (square at a different orientation) with the positive field shown as solid contours. The long dashed line sketches the Hα surge (s)

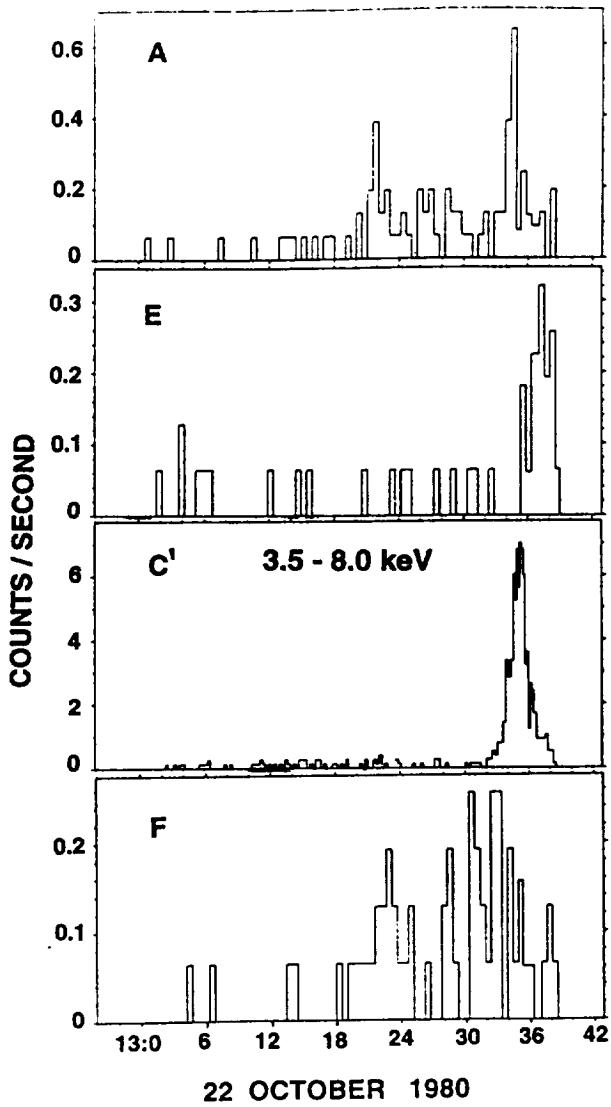

Fig. 9. 3.5–5.5 keV X-ray emission for the points A, E, C′ and F on October 22 1980. The time history suggests an impulsive energy release linking A, C′ and F, then E

The X-ray data show that both active regions were involved in the events leading up to the surge activity. Early in the event, say before 13:25 UT, the emissions from A and F were comparable; then at 13:30 UT F dominates. This then appears to have triggered the energy release from A, in AR 2748, which was followed within 30–60 s by the main event from C′. The distance between A and C′ was around 150 000 km, corresponding to the angular separation of 3′. The inferred velocity is then 3000–1500 km s^{-1}. Disturbance velocities of this magnitude have been observed before for closely separated events from adjacent active regions (Doyle et al. 1985; Simnett et al. 1990). Points C′ and F were on opposite sides of a region of negative polarity in AR 2744, and both projected on the neutral line. The behaviour of the X-ray emission suggests that there was a complex magnetic loop structure, associated with impulsive energy release, linking A, C′ and F. The onset of the emission from E precisely (to within the 15s resolution of the data) at the same time as the emission from C started to fall, also provides evidence for a link between E and the other points.

The emission measure EM and the temperature can be calculated for the flare from C′. Table 4 shows the evolution versus time of the EM in X rays. The X-ray burst from region C′ did not exhibit a uniform temperature, and we have broken it into four time intervals. We have analysed the emission to give a two-temperature fit, wherever this is possible. The data do not have sufficient resolution for a differential emission measure analysis to be performed. For the onset phase, there was a distinct very high temperature component of 32 10^6 K, together with a lower temperature component at 13.4 10^6 K. As the soft X-ray intensity approached maximum, both derived temperatures dropped slightly. However, the emission measure increased dramatically for the low temperature component, and by a factor of 2.5 for the high temperature component. As the plasma temperature dropped, the derived emission measure increased. In the final stages of the decay, the high temperature component was still present. During the initial part of the decay, the best fit gives a low temperature component of 11.6 10^6 K, and as the flare decayed the temperature cooled to 7.8 10^6 K. It is probably an artefact of the analysis that the emission measure appears to drop around 13:35 UT to 2.5 10^{47} cm^{-3}; this is a consequence of a high count in the 5.5–8.0 keV channel. If this count is reduced by

Table 4. The temperature and emission measure for the event from region C′

Time interval	T 10^6 K	EM (cm^{-3})
13:32:43–13:33:52	32.0	$1.4\ 10^{45}$
	13.4	$2.0\ 10^{46}$
13:34:43–13:34:56	25.5	$3.6\ 10^{45}$
	9.1	$4.1\ 10^{47}$
13:34:58–13:35:27	24	$3\ 10^{45}$
	11.6	$2.5\ 10^{47}$
13:35:29–13:37:18	24	$3\ 10^{45}$
	7.8	$4.3\ 10^{47}$

1σ then the temperature for the best fit goes down to $10.7\ 10^6$ K and the emission measure increases to $3.3\ 10^{47}\ cm^{-3}$.

The main result from this analysis is that apart from a relatively constant, but low level, component at a high temperature, the additional response from the flare is well fitted by a plasma temperature in the range 9–11 10^6 K with an emission measure around $4\ 10^{47}\ cm^{-3}$. The plasma cooled to below $8\ 10^6$ K within around one minute of the peak intensity.

5. Energy budget for the surge on October 22

5.1. Kinetic energy

Kovács & Dezsö (1990) calculated the kinetic energy taking into account the measured velocity of ejection and an estimate of the amount of ejected mass. The kinetic energy was of the order of 10^{28} to 10^{29} erg for an electron density of 10^{11}–$10^{12}\ cm^{-3}$ which are commonly used values at $T \sim 10^4$ K.

5.2. Energy in the X-ray emitting plasma

Unfortunately the flare occurred outside the HXIS fine field of view so that a good estimate of the volume is not available. However, it is possible to make an estimate of the volume by considering the C IV images:

$$V = WAL$$

with W the filling factor, A the area of the subflare = $1.5\ 10^{17}\ cm^{-2}$, L the length of the surge, equal to $2\ 10^9$ cm.

$$V \sim W \times 3 \times 10^{26}\ cm^3$$

The electron density can be derived as following:

$$n_e = \sqrt{EM/V} = \sqrt{EM/(W \times 3 \times 10^{26})}$$

With $EM = 4\ 10^{47}\ cm^{-3}$ results $n_e = 3\ 10^{10}/\sqrt{W}\ cm^{-3}$, i.e., the total gas pressure would be $75/\sqrt{W}$ dyne cm^{-2}.

The energy Q is equal to

$$Q = 3\,k\,T\,n_e\,V = 3\,EM\,k\,T/n_e.$$

From the analysis of the X-ray data the emission measure and the temperature may be calculated. The temperature analysis is subject to systematic uncertainties, primarily because the differential emission measure cannot be determined by HXIS, and consequently the plasma has to be characterised by at best two components. This situation is somewhat artificial but it does provide an indication of the general nature of the high temperature plasma. It is evident from Table 4 that for this small flare the contribution to the emission from the high temperature component was small. Therefore in the energy estimate we have neglected it in favour of the dominant low temperature component.

With $T = 10^7$ K, $Q \sim 4\ 10^{28}\sqrt{W}$

If $W = 1$, $Q \sim 4\ 10^{28}$ erg s, this is a upper limit, if $W = 0.01$, $Q \sim 4\ 10^{27}$ erg s and $n_e \sim 3\ 10^{11}\ cm^{-3}$.

5.3. Energy in the C IV-emitting plasma

5.3.1. For the surges

To obtain a value of the emission measure for the surge we considered the third C IV image of experiment No.14195. In this image we were able to identify a loop structure extending towards the southwest of the subflare which was associated with the Hα surge. Taking a mean value for the number of counts in pixels that we assume belong to the *surge* we obtain a mean intensity I_{ob} of $2.5\ 10^4$ erg $cm^{-2}\ s^{-1}\ sr^{-1}$. According to Raymond & Doyle (1981) Eq. (3);

$$N_e^2 \delta h = I_{ob}/I_{pr}\ 10^{26}\ cm^{-5}$$

where the values of I_{pr} are taken from their Table 2, δh is the height over which the C IV is emitting. There is some slight variation of these results for different values of electron pressure but this is not very important for our present discussion. We obtain:

$$SEM = 6.1\ 10^{26}\ cm^{-5}$$

where SEM is the emission meassure per unit area. The area of the surges observed in C IV is $A \sim 8\ 10^{17}\ cm^2$ resulting in a total emission measure of $4.9\ 10^{44}\ cm^{-3}$. This is much less than the total X-ray emission measure in the X-ray flare. The duration can be estimated as 2000 s.

If we consider an electron pressure, P_e, that is consistent with typical values and with those used above, e.g., P_e = 30 dyne cm^{-2} ($n_e \sim 10^{12}\ cm^{-3}$), we can estimate the dimension of the emitting C IV plasma within each pixel. Assuming that the surge material took the form of a loop with cylindrical cross-section and that it extended for much more than one pixel (i.e., the loop has a constant cross-section within a pixel), the loop diameter can be estimated to have been about 40 km. (i.e., 1/20″). A number of loops may have existed and then their accumulated dimension within a pixel, if distributed uniformly, would have been 40 km.

The thermal energy content in this plasma is only $2\ 10^{22}$ erg, 10^{-6} times the energy in the X-ray flare. This estimate is based on an electron density of $n_e \sim 10^{12}\ cm^{-3}$. However, the energy radiated at transition region temperatures is substantial and the

C IV radiative losses resulting directly from the observed intensity are about 5 10^{26} erg. It is clear that the material is not heated first to 10^5 K, then cools down by radiation. A part of the radiated energy should come directly from X-ray hot plasma by conduction or directly from mechanical energy. Using the Cox & Tucker (1969) function and the total emission measure and duration of the event we infer total losses of $\sim$ 1 10^{27} erg for all the plasma at T 10^5 K. This energy is of the order of than that contained in the flare X-ray plasma (see Sect. 5.2) and is a consequence of the high radiative efficiency of the transition-region type plasma compared to the X-ray plasma.

5.3.2. For the subflares

The maximum values of the C IV intensity for each of the three subflares are: 8.7, 7.2 and 6.6 in units of 10^5 erg cm^{-2} s^{-1} sr^{-1}. These values are very similar and we use the mean intensity from the three brightest pixels of the second image in the experiment No.14195. These give an apparent area A$\sim$ 1.5 10^{17} cm^{-2}. The duration of the brightening can be estimated from the Hα data as $\sim$ 200 s. Using the mean intensity value and the previous procedure we estimate an emission measure SEM_{RD} (according to the Raymond and Doyle definition) of 1.7 10^{28} cm^{-5}. When we multiply by the area observed in C IV we get 2.5 10^{45} cm^{-3} which is two orders of magnitude smaller than the X-ray flare value (see Table 4). We can estimate not only the radiative losses from the C IV emitting plasma but also, using the FAL results (Fontenla et al. 1991b), the losses from the cooler material that emits Lyα. To do this we assume that the observed C IV bright pixels are the footpoints of hot loops. This assumption is fully consistent with all the data we examined. The definition of emission measure by FAL is different from that by Raymond & Doyle (1981), so that

$$SEM_{FAL} = n_e n_H (\mathrm{d}(\ln T)/\mathrm{d}z)^{-1} .$$

Thus, SEM_{FAL}=4.34 SEM_{RD} and the corresponding value for the subflare is EM_{FAL}=7.9 10^{28} cm^{-5}. Using FAL Eq. (17), we find that the total gas pressure required for radiating away the heat flux implied by this emission measure is p = 320 dyne cm^{-2}. Comparing this with the estimate from X-rays we find that if pressure equilibrium existed (viz. the X-ray and UV pressure were the same), the filling factor W (see Sect. 5.2) should be W = 0.056.

Then, using FAL Eq. (16) we obtain a very steep temperature gradient at the Lyα-emitting region,

$$\mathrm{d}(\ln T)/\mathrm{d}(\ln z) = 1.7\ 10^{-3} .$$

However, because of the large density of this region, $n_e \sim 10^{13}$ cm^{-3}, it must occur deep in the chromosphere and the electron mean free path is substantially smaller that the inverse of the temperature gradient. Using FAL Eq. (15) we obtain a total heat flux of $F_H \sim 5.5\ 10^8$ erg cm^{-2} s^{-1}. This, together with the apparent area and the duration give a total radiative loss of $RE \sim 1.6\ 10^{28}$ erg. In this calculation we have assumed that the total heat flux is constant in the hotter part of the transition region at the footpoint of the X-ray loops. This may not be totally accurate for the high pressure that we consider here. Using the arguments previously used for the surges, we conclude that the radiative losses by the hotter part of the transition region would be also $\sim$1.6 10^{28} erg. Thus, we conclude that in the subflares probably the radiative losses at $T \sim 10^5$ K are similar to those in Lyα and He lines, and the total losses are about 3 10^{28} erg. This energy is about one order of magnitude larger than that of the surges. The radiative losses are about 3 times larger than the estimate of the total energy in the X-ray plasma (Sect. 5.2), when the dilution or filling factor W = 0.056 is taken into account. This would exclude the possiblity that the energy radiated resulted from the cooling of plasma suddenly heated to 10^7 K in the way that has been proposed for large flares. Rather, continuous energy input was necessary to sustain the event throughout its whole duration (of course a number of elementary releases spread in time and/or in space could also do it). In an extreme limit of unity filling factor W = 1, the UV radiative losses would be comparable with the X-ray plasma energy, but this is unlikely.

The extent along the line of sight where the C IV material existed can be related to the emission measure by the equation

$$LW_{UV} = SEM_{RD}/n_e^2$$

where

$$L^{-1} = \mathrm{d}(\ln T)/\mathrm{d}(\ln z)$$

and W_{UV} is a "filling factor" (different from the X-rays case) that relates the actual area that was filled by emitting C IV to the apparent area of the observed material (in our case the pixel area). For the subflares, the steep temperature gradient leads to a very small value, $L \sim$ 6 m, and the very high pressure leads to an electron density of 10^{13} cm^{-3}, which is compatible with the emission measure for dilution factor W_{UV} = 1. The only possible way to obtain a larger L would be to assume a smaller electron density, but this seems unlikely. Moreover, if a smaller electron density is assumed it would be hard to explain why the higher pressure hot plasma did not collapse the transition region, and the only way would be to assume a smaller pressure also for the hot component. Assuming a lower density would give a number of problems for explaining the observations; therefore, we conclude that the most likely is that the values we give are realistic and that the actual thickness of the C IV emitting material was really very small.

6. Discussion

We have analysed subflares and surges occurring on October 21 and 22 1980 observed in multi-wavelengths during the SMM mission. We have compared what we need to balance the kinetic and potential energy losses and what emission measure we have in C IV and in X-rays. In the main events, if the subflare is physically related to the surge the X-ray emission is sufficient to support either of the two models, namely a gradient pressure mechanism, as first suggested by Steinolfson et al (1979), or a magnetic reconnection process. This arises because the range

of available variable parameters is too large for observations of spatial resolution of a few arcseconds to provide sufficient constraints on any particular model. Here we briefly outline the problem.

6.1. Gradient pressure driven model

The atmospheric response to rapid energy deposition at a given layer will be to induce a pressure pulse which will drive the overlying material upwards and possibly the underlying material downwards. If the energy input to the chromosphere is from non-thermal particles accelerated in the overlying region, then filamentation of the particle beam will occur. Current measurements do not have the resolution to address this, but it may be inferred from considerations of the filling factor that the dimensions of a given channel are considerably less than 1″, and probably less than 10^{-2}″.

Sterling et al. (1993) have presented the results of a series of numerical simulations where they considered energy input, by an unspecified process, to various depths of the chromosphere at amounts ranging from 5 10^{24} to 5 10^{28} ergs. They found that the resulting emission depended critically both on the depth of the energy deposit and on the magnitude of the deposit. They were able to produce simple pressure gradient jets, two component jets, where one component is a pressure gradient jet, and the other is a cool, shock generated jet, and gas plugs. Gas plugs form when the energy deposition is in a very narrow portion of the chromosphere.

If we accept the results of Sterling et al. (1993), and also the deductions of filamentation, then it is clear that we are faced with a currently insurmountable inversion problem. However, we are able to state that continuous input of energy is necessary to sustain the event during its long duration (30 min). Depending on the energy flux in a given filament and the depth at which the majority of the energy is deposited, then plasmas of varying temperatures from 10^4 K to over 10^6 K can be produced. There is support for the pressure gradient model from the concept of energy tranfer by ions beams suggested by Simnett (1986), as an accelerated ion spectrum with a peak in the energy spectrum similar to that detected by Armstrong et al. (1994) from a coronal event will deposit much of its energy in a relatively narrow band of the chromosphere. Filamentation can then produce a variety of the conditions modelled by Sterling et al..

6.2. Reconnection model

Given that our observations could match a variety of the possible scenarios discussed by Sterling et al. (1993) for completeness we now examine the situation for magnetic reconnection. Forbes (private communication) agreed that reconnection still looks promising as a mechanism for surges. We think that for a reconnection model, the heat energy which is released (nkT) should always be at least 50% of the kinetic energy which is observed ($0.5\rho v^2$). As we have already argued, the amount of X-ray emission will depend on the temperature which in turn depends on the density. For a high density plasma like the chromosphere or transition zone, the temperature may be sufficiently low that only a small amount of X-ray emission occurs. However, the heating is still there, so if one looks at lower temperatures like C IV, then more emission should be present than in X-rays. This is consistent with our results, where we have a one order-of-magnitude difference between the 10^5 K emission measure and the 10^7 K emission measure.

The magnetic energy stored is transferred directly to kinetic energy of cool plasma, with the high temperatures characteristic of flares not being attained. A small amount of it is visible in thermal energy as we have demonstrated by looking at the energy content in the 10^4 to 10^7 K plasma. Some of the magnetic energy may be transferred to non thermal electrons such as those responsible for the simultaneous type III radio bursts. It appears that the release is not impulsive but progressive and could last at least 200 s.

Acknowledgements. We thank Drs. T.G. Forbes and P. Démoulin for fruitful discussions, Drs. A. Kovács and Dezsö for providing images in Hα from Debrecen, Dr. M. Hagyard for the MSFC magnetogram. The MSDP data were analysed by the microdensitometer of Paris (MAMA). This study has been partially funded by the contract NSF-CNRS between the University of Huntsville and the DASOP (Observatory of Paris). The HXIS data analysis was supported by the SERC.

References

Armstrong T.P., Haggerty D., Lanzerotti L.J., et al., 1994, Geophys. Res. Lett. 21, 1747
Chiuderi-Drago F., Mein N., Pick M., 1986, Solar Phys. 103, 235
Cox D.P., Tucker W.H., 1969, ApJ 157, 1157
Démoulin P., Mandrini C.H., Rovira M.G., et al., 1994, Solar Phys. 150, 221
Doyle J.G, Byrne P.B., Dennis B.R., et al., 1985, Solar Phys. 98, 141
Fontenla J.M., Švestka Z., Farnik F., Tang F.Y., 1991a, Solar Phys. 134, 145
Fontenla J.M., Avrett E.H., Loeser L.R., 1991b, ApJ 377, 712 (FAL)
Heyvaerts J., Priest E.R., Rust D.M., 1977, ApJ 216, 123
Kovács A., Dezsö L., 1990, Solar Phys. 129, 313
Kovács A., Dezsö L., 1988, Proceedings of Irkutsk SMY Workshop, Eds Obridko V.N., Smolkov G., 317
Mandrini C.H., Rovira M.G., Démoulin P., et al., 1993, A&A 272, 609
Martin S.F., Švestka Z., 1988, Solar Phys. 116, 91
Raymond J.C., Doyle J.G., 1981, ApJ 245, 1141
Schmieder B., Vial J.C., Mein P., Tandberg-Hanssen E., 1983, A&A 127, 337
Schmieder B., van Driel-Gesztelyi L., Gerlei O., Simnett G.M., 1993, Solar Phys. 146, 163
Schmieder B., Golub L., Antiochos S.K., 1994, ApJ 425, 326
Schmieder B., Shibata K., van Driel-Gesztelyi L., Freeland S., 1995, Solar Phys. 156, 245
Shibata K., Ishido Y., Acton L.W. et al., 1992a, PASJ 44, L173
Shibata K., Nozawa S., Matsumoto R., 1992b, PASJ 44, 265
Simnett G.M., 1986, Solar Phys. 106, 165
Simnett G.M., Sotirovsky P., Simon G., 1990, A&A 227, 235
Solar Geophysical Data, 1980, No. 436, Part I, 151
Steinolfson R.S., Schmahl E.J., Wu S.T., 1979, Solar Phys. 63, 187
Sterling A.C., Shibata K., Mariska J.T., 1993, ApJ 407, , 778
van Driel-Gesztelyi L., Hofmann A., Démoulin P., Schmieder B., Csepura G., 1994, Solar Phys. 149, 309